

Modeling and Investigation of Interfacial Interaction between PLA and One Type of Deficient Hydroxyapatite

Tao Guo, Shaobing Zhou,* Xiaotong Zheng, and Jing Jiang

School of Materials Science and Engineering, Key Laboratory of Advanced Technologies of Materials, Ministry of Education, Southwest Jiaotong University, Chengdu 610031, People's Republic of China

Received: February 24, 2009; Revised Manuscript Received: May 24, 2009

A model of one type of deficient hydroxyapatite (D-HA) was constructed, and the interaction mechanism between polylactide acid (PLA) and the (001) surface of D-HA was also investigated for the first time employing density functional theory (DFT) in the Perdew, Burke, and Ernzerhof (PBE) generalized gradient approximation (GGA). First, a mathematical model of D-HA was abstracted from experimental facts, through which a group of special values and the nonstoichiometric formula, $\text{Ca}_8[(\text{HPO}_4)_3(\text{PO}_4)_2(\text{CO}_3)](\text{OH})_2$, were obtained. Next, a stable configuration of D-HA was achieved with the method of searching stable structure gradually. After the most stable configuration was identified, our attention mainly turns to the results concerning the (001) surface of D-HA. Methyl lactate was employed to act as PLA monomer estimating the interaction behavior between PLA and D-HA. Simultaneously, to achieve an accurate description of hydrogen bonds (hbs), a plane wave energy cutoff of 700 eV was used. Significantly, we observed that there were two P—OHs on the surface, but only one can form a hydrogen bond with PLA; also, besides the interaction between carbonyl oxygen ($\text{C}=\text{O}$) in the PLA and calcium ions in the D-HA, there are two kinds of hbs interactions: one type is the medium stronger hbs between the $\text{C}=\text{O}$ and the hydrogen in HPO_4^{2-} with the bond length of 1.69 Å and bond energy of about 48 kJ mol⁻¹; the other is the weak hbs between the oxygen in phosphate and the hydrogen in methyl/methylene with the average bond length of about 2.48 Å and bond energy of about 9 kJ mol⁻¹. PDOS was also employed to characterize the existence of hbs. Our results may have potential promotion to investigate the properties of polymeric nanocomposites.

Introduction

Polymer matrix nanocomposites consist of polymer and nanoparticulate, which play an important role in many fields, such as clinical, aerospace, automotive, marine, military, and infrastructure.^{1,2} In these fields, the primary disadvantages in single materials have been avoided. Moreover, some new and/or improved properties (strength, stiffness, toughness, etc.) can be obtained,^{3–5} mainly due to the high surface area resulting in intense interactions between the polymer matrix and the nanofillers.² Furthermore, hydroxyapatite (HA) filled nanocomposites as biomaterials due to its high mechanical properties,^{6,7} favorable biodegradation,⁸ and excellent biocompatibility⁹ have been used clinically in various forms.^{10,11} Moreover, recently our research group even found HA nanofillers could effectively improve shape memory properties of polylactide acid (PLA) in PLA/HA nanocomposites.³ Whereas, how are the interactions between organic and HA surfaces produced in nanocomposites? To make the question clear, the physicochemical as well as the surface properties of HA have been extensively investigated by some groups, such as Tanaka et al.¹² and Cheng et al.¹³ However, until recently the explanation for the interaction mechanism between polymer matrix and HA is still controversial. Wang et al.¹⁴ and Nikolenko et al.¹⁵ have suggested both the P—OH and the Ca^{2+} were the adsorption centers. Nikolenko et al.¹⁶ also noted that the Ca^{2+} did not participate in the surface interaction in another condition before. Misra thought that not P—OH but Ca^{2+} was the active site.¹⁷ Pasteris et al.¹⁸ proposed that the OH⁻ in apatite of animals bone could affect the interaction and

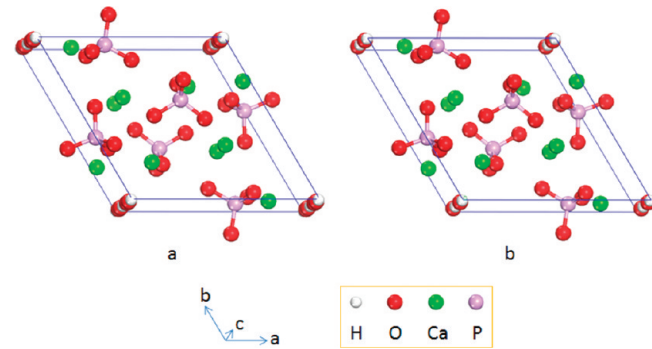


Figure 1. Plane view of hydroxyapatite unit cell. Structure a is derived from the X-ray data given in ref 9. This structure is in the $P6_3/m$ space group, which exhibits an intrinsic disorder in the hydroxyl ion location. This disorder results in doubling of the amount of the hydroxyl ions per unit cell. Structure b is optimized using DFT methods with the implementation of full periodic boundary conditions. This structure is in the $P1$ space group after removing excess OH groups.

solubility and so on. Hence, the adsorption mechanism of organic phase onto HA is a valuable research issue.

It is well-known that pure HA [$\text{Ca}_{10}(\text{PO}_4)_6(\text{OH})_2$] has a hexagonal structure with space group $P6_3/m$ and lattice parameters $a = b = 9.4225$ Å, $c = 6.8850$ Å.¹⁹ As shown in Figure 1a, calcium ions are located in two different sites: Ca(I) is coordinated to nine oxygen ions situated in six different phosphate tetrahedron, and Ca(II) is 7-fold coordinated by six oxygen ions of five phosphate groups and the hydroxyl ion. The Ca(II) are distributed in a hexagonal screw configuration along the c-axes, forming tunnels whose center is occupied by

* Corresponding author. Phone: 86-28-87634023. Fax: 86-28-8764649. E-mail: shaobingzhou@swjtu.edu.cn, shaobingzhou@hotmail.com.

an array of hydroxyl ions. This HA structure has a disordered hydroxyl arrangement along the *c*-axis, and the hydroxyl ions are pointed in upper and lower directions (in statistical fashion) against the mirror planes at $z = 1/4$ and $z = 3/4$.²⁰ Monoclinic structures have also been reported,^{21,22} which are obtained from the hexagonal one by doubling the *b* lattice parameter with four formula units per unit cell. In the monoclinic unit cell, hydroxyl ions are aligned in the same direction along the *c*-axis and are antiparallel in adjacent columns.

Most of the HA synthesized in air from aqueous system by precipitation or hydrolysis methods and contained in biological hard tissues are nonstoichiometric materials. In the synthesis process, due to the alkaline conditions, CO₂ in atmosphere is very easy to incorporate into apatites.²³ Also, most of the biological apatites contain several other ions, mainly carbonate (CO₃²⁻) and traces of Na⁺, Mg²⁺, Fe²⁺, Cl⁻, HPO₄²⁻, and F⁻.^{24,25} On the basis of all of the above facts, HA with deficient structure has been studied extensively in theory and practice. For example, Suetsugu et al.²⁶ and Peroos et al.²⁷ have studied the CO₃²⁻ location details in A-type substitution from experiment and theory, respectively. However, B-type substitution is more important^{23,28} and has caused more attention. Wilson et al.²⁹ suggested that the CO₃²⁻ occupied randomly one of the mirror symmetry related faces of a vacated PO₄³⁻ site with the normal to the CO₃²⁻ plane of about 30° to the *c*-axis, studying a sodium-containing synthetic carbonate HA structure (CO₃²⁻ content 12.5 wt %). Ivanova et al.³⁰ studied a HA structural model with 4.4 wt % CO₃²⁻ content and proposed the CO₃²⁻ randomly occupy the adjacent faces of a substituted phosphate tetrahedron and be parallel to the *c*-axis. The charge compensation caused by CO₃²⁻ replacing PO₄³⁻ groups is primarily by vacancies in Ca(I) sites. Fleet et al.³¹ reported on the location of B-type CO₃²⁻ in a Na-bearing type A-B carbonate apatite single crystal. According to the authors, it is located closely to the sloping faces of the substituted phosphate tetrahedron, but is inclined at an angle of 53° to the mirror plane. In a neutron powder diffraction study, a substitution on the mirror plane of the phosphate tetrahedron was also proposed by Leventouri et al.³² Astala et al.³³ have studied different carbonate substitution mechanisms in bulk hydroxyapatite by means of first principles simulations. A single B-type CO₃²⁻ substitution configuration with one H atom placed at one Ca vacancy for charge compensation was also studied. According to the authors, the CO₃²⁻ plane was close to parallel to the (001) crystal plane, making an angle of about 4° with it. Peroos et al.²⁷ employed computer modeling techniques to investigate the uptake and distribution of substitutional CO₃²⁻ groups in the HA lattice. One B-type deficient structure was studied with one of the Ca²⁺ ions near the substitution carbonate group being replaced by one K⁺ ion. They denoted that in the lowest energy structure, the CO₃²⁻ group was lying almost flat in the *a/b*-plane of the apatite lattice with a small angle of about 15° to the *c*-axis.

Currently, molecular simulation provides many new significant insights into the understanding of organic adsorption on nanoscale surfaces at the atomic level. It has become one of the most direct approaches to theoretically investigate the atomic details of surface interaction in the polymeric nanocomposites. On account of deficient HA (D-HA) surface having a higher activity than pure HA,^{13,28,34} it is more reasonable to construct a D-HA surface structure on studying the interaction between organic phase and D-HA than pure HA. To make the D-HA model surface closer to the fact, a more realistic charge compensation mechanism and lower surface energy of configuration on the D-HA surface are essential. On the basis of the

above considerations, we will first build a mathematical model describing the charge compensation mechanism based on the experimental fact. Next, we select a stable D-HA model according to a special case derived from the former mathematical model. We then mainly study a hydrogen-bond (hbs) interaction between simplified PLA model and the surface of D-HA model, with a view to provide helpful strategies for studying the interaction between organic phase and nanosurfaces.

Experimental Section

Computational Methodology. The CASTEP (Cambridge Serial Total Energy Package) program module in Materials Studio (MS) 4.2 software of Accelrys Inc. was employed to implement almost all of the model calculations in this study. Generalized gradient approximation (GGA) was adopted for the exchange-correlation interaction, and Perdew–Burke–Ernzerhof (PBE) parametrization was used for the GGA exchange-correlation potential.³⁵ Ultrasoft pseudopotentials were used to describe the electron–ion interactions. The electronic wave functions were obtained using a density-mixing scheme,³⁶ and the structures were relaxed using the Broyden–Fletcher–Goldfarb–Shannon (BFGS) method.³⁷ Self-consistent field (SCF) electronic structure calculations were conducted with a convergence tolerance of 5×10^{-7} eV/atom. The Kohn–Sham orbitals were expanded with a plane wave energy cutoff of 700 eV in hbs study and 380 eV in the CASTEP study. Brillouin zone sampling was performed using the Monkhost–Pack scheme with a Γ *k*-point in model selection, $2 \times 2 \times 2$ *k*-point in the final defect structure relaxation, and $2 \times 2 \times 1$ in the surface study. In all CASTEP calculations, the total energy of the system converged to less than 5×10^{-6} eV, the residual force to less than 0.01 eV/Å, the displacement of atoms to less than 5×10^{-4} Å, and the residual bulk stress to less than 0.02 GPa. When dealing with PLA model, we first use the Discover program module in MS to pretreat it, in which the COMPASS force field is employed with nonbond cutoff distance of 15.50 Å, spline width of 5.00 Å, and buffer width of 2.00 Å, respectively; we then utilize CASTEP to perform the following geometry optimization.

D-HA Geometry. The CASTEP program module in MS cannot be used to describe the structure of HA derived from the X-ray data given by Kay et al.,¹⁹ and it is more time-consuming to deal with the monoclinic structures²¹ by employing CASTEP. So we used the supercell of hexagonal HA structure (44 atoms) without applying any symmetry (*P*1) and removed the excess OH⁻ groups,^{38,39} as seen in Figure 1b. The HA particles will mainly cleave along surfaces that have large interplanar spacings and few interplanar bonds, usually low-index surfaces with low surface energies under dry conditions. It was shown from both experiments and theoretical calculations that the (001) surfaces of apatite are the most stable interfaces with respect to vacuum and aqueous phases⁴⁰ and have also been used as the main interaction interfaces in much literature.^{41–44} Here, we also employed the (001) surface of D-HA as the interaction interface. According to the results of Zhu et al.,⁴⁵ the vacuum width of 12.0 Å was enough to obtain meaningful results, and a two-layer slab (about 15.6 Å) as the minimum thickness was needed to obtain meaningful results. During the relaxation of the (001) surface, we used the same vacuum width and a similar but not the same two-layer slab. In this Article, the vacuum width of about 12.0 Å was used in surface relaxation, around 18.0 Å was used in adsorption study, and a slab thickness of 2 layers (about 13.6 Å) was used in all of the calculations with the bottom atoms in the box fixed. A single

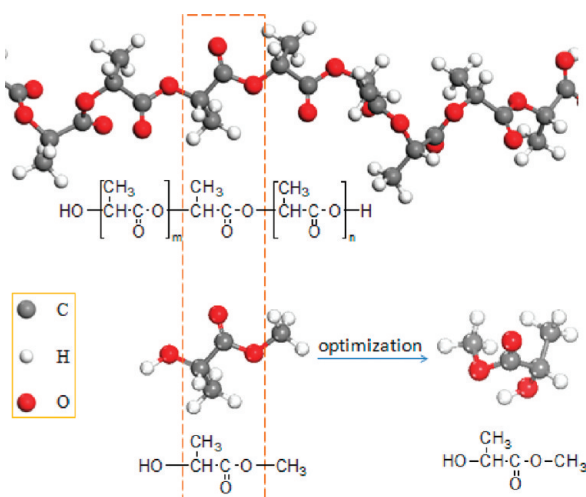


Figure 2. Schematic diagram of obtaining PLA model (methyl lactate) from PLA.

cell surface area was used in the adsorption research. The accuracy of this size is somewhat suspected because of the possibility of spurious interactions between periodic images. However, it is unlikely that any such errors would change the qualitative result that there is a large energy penalty for separating C=O from the vicinity. Also, in the following, this effect is very small according to our test.

PLA Model. Here, methyl lactate was used to act as PLA monomer for estimating the interaction behavior between PLA and D-HA. Its purpose is to strike a balance between the calculation accuracy and efficiency. The methyl lactate can be seen as one monomer of PLA intercepted and then terminated by methyl and hydroxyl, as illustrated in Figure 2. This can further reduce the differences between the repeating unit of PLA and the corresponding parts in methyl lactate, especially the functional groups of carbonyl oxygen. Also, at the same time, the target system is not too large. To make the errors unambiguous, we also give the difference of C=O in methyl lactate and in PLA (12 monomers). The Mulliken charges are $-0.41e$ and $-0.39e$, respectively. The electrostatic potentials are $-0.45e$ and $-0.44e$, respectively. The data of PLA (12 monomers) are the average value of the middle four C=O. Therefore, the methyl lactate used to act as PLA may slightly overestimate some properties, such as the binding energy, etc. The crude methyl lactate structure had been treated by the Discover module in MS at first: The crude methyl lactate was initially minimized, and then Molecular Dynamics (MD) simulations were performed for 50 ps at 300 K. Furthermore, the temperature was increased to 500 K and brought back to 300 K with steps of 50 K. For each temperature, MD simulations were performed using the NVT ensemble for a total time of 50 ps. Next, the model was minimized. The treated methyl lactate model by Discover module was then put into a vacuum orthorhombic box with the side length of 30 Å to perform geometry optimization using CASTEP module in MS software. The obtained PLA model will be used in the subsequent calculations.

D-HA Model. Determining the Number of Atom/Atoms at Corresponding Places in Each Primitive Cell. Most HA synthesized using precipitation or hydrolysis methods and in organism contains mainly CO_3^{2-} impurity ions.^{26,46} It is now generally accepted that the principal possible sites for CO_3^{2-} ions substitution are A-type and B-type.²³ Also, in most high-temperature apatite, the CO_3^{2-} ions are easily resident in the form of A-type substitution, whereas in the low-temperature

materials the CO_3^{2-} ions easily form a B-type substitution.³³ Also, at low temperature the compositions of synthesized HA are similar to bone.⁴⁷ For the reason of CO_3^{2-} ions substitution, the apatite is also concomitant with Ca deficient.^{13,23} There is also experimental evidence of HPO_4^{2-} groups in carbonate HA acting as compensating species,^{3,48–50} and little OH vacancy in some synthesized HA.³ We also notice that OH^- ions vacancy and substitution by CO_3^{2-} ions are not conducive for obtaining more HPO_4^{2-} ions in the maximum extent of the charge compensation being considered in D-HA.

On the basis of the facts above and considering the demands in this study as well as the calculation time assurer, we made the following assumptions: CO_3^{2-} ions are the only impurity ions in the D-HA model; there is no OH vacancy and A-type carbonate substitution but only B-type substitution in D-HA lattice; and the charge compensation takes place only by calcium vacancies and hydrogen atoms bonding to phosphates to form HPO_4^{2-} ions. To embody the problem, in each D-HA primitive cell, we made V as the number of Ca vacancy; F as the number of HPO_4^{2-} ; S as the number of B-type CO_3^{2-} substitution; the Ca/P molar ratio equal to R ; the mass contents of CO_3^{2-} equal to W ; and the charge in each primitive cell is C . We then obtained eq 1.

$$\begin{aligned} 2(10 - V) - 1 \times 2 - 2(F + S) - 3(6 - F - S) &= C \\ \frac{10 - V}{6 - S} &= R \\ \frac{60S}{40(10 - V) + 95(6 - S) + 60S + F + 17 \times 2} &= W \end{aligned} \quad (1)$$

If all of the variables in the current circumstances are meaningful, to solve it, we can achieve the following results, eq 2:

$$\begin{aligned} V &= \frac{120(3W + 5) + R[W(C + 788) - 360]}{W(38R + 36) + 60} \\ F &= \frac{60(C - 12R + 20) + W[1348R + 5C(8R + 7) + 96]}{W(38R + 36) + 60} \\ S &= \frac{W(C + 228R + 624)}{W(38R + 36) + 60} \end{aligned} \quad (2)$$

It was reported that CO_3^{2-} contents in synthesized HA fluctuate from 0.09 to 12.5 wt %,^{51–53} also in animal HA with contents of 2–8 wt %,^{54–56} most synthesized HA was with a Ca/P molar ratio from 1.50 to 1.67.²³ To make our calculation provide more practical meaning, we select a group of specific values in experiment. We made $W = 6.726$ wt %, $P = 1.60$, and $C = 0$ to maintain the charge neutrality. These values can also make the scale of D-HA smaller. The following results are then achieved, eq 3:

$$\begin{aligned} V &= 2 \\ F &= 3 \\ S &= 1 \end{aligned} \quad (3)$$

From now on, the number of atom/atomic group in corresponding locations in each D-HA cell has been ascertained, and the molecular formula is $\text{Ca}_8[(\text{HPO}_4)_3(\text{PO}_4)_2(\text{CO}_3)](\text{OH})_2$. Also, if we do not consider the Ca/P molar ratio and the concentration of CO_3^{2-} , we can obtain the following sum formula: $\text{Ca}_{10-(x+y)/2}[(\text{HPO}_4)_x(\text{PO}_4)_{6-x-y}(\text{CO}_3)_y](\text{OH})_2$, with $x \geq 0$, $y \geq 0$,

and $x + y \leq 6$. This form is the same as the form in the literature.^{23,31,50}

Steps of Constructing D-HA Structure. Here, we will construct a D-HA model based on the molecular formula $\text{Ca}_8[(\text{HPO}_4)_3(\text{PO}_4)_2(\text{CO}_3)](\text{OH})_2$ described above. To add/substitute the foreign atoms/atomic groups to/in pure HA/D-HA lattice more reasonably, we utilize a method similar to that of Calderín⁵⁷ and Astala et al.³³ In the following, we will accord to the order that: CO_3 substitute for $\text{PO}_4 \rightarrow$ delete Ca \rightarrow add H \rightarrow delete Ca \rightarrow add H \rightarrow add H. To make it more strict and well-founded that the energy is the lowest in final configuration, we first make three assumptions as follows:

(I) The introduced defect impacts the relative position of the atoms in the last structure slightly and is not enough to remodel the status of the atoms in the former lattice (i.e., Ca, O... are near their former sites; O is bonding to P...; Ca(I) and Ca(II) are all of the same status as the former...).

(II) We presume that the pure HA is the most stable structure because the point defects concentration is superfluous and the temperature is 0 K in our calculation, although the crystal lattice containing a certain concentration of point defects is the most stable structure. Therefore, the lattice structure that is in favor of maintaining this structure is a more stable structure.

(III) There is no relatively higher energy barrier, and the transition is smooth during all of the optimization process.

In fact, according to the theory of crystallography, if the charge, size, etc., of impurity atoms/atomic groups or vacancy deviate not too much from the original, and the concentration of these impurity particles/vacancy is low, in most cases the upper assumptions are feasible and reliable to abide by. Unfortunately, we cannot give an accurate attestation here. On the basis of assumptions I and III, we can conclude that it is almost impossible that a certain structure in current step building on the metastable structure in the last step is a more stable structure in the process of constructing D-HA. That is to say, to a certain extent, we can obtain the final stable structure through constructing the most stable structure in each step. In this regard, we can take the stable structure in the last step for a pure HA structure approximately and focus on selecting the most stable structure in every step. As a result, we have divided a stability problem of complex doping structure into a number of stability problems of simple doping structures.

From the analysis above and assumption II, we can derive the following three principles:

(I) When deleting an atom, we select the atom that is most impacted by the introduction of defects in the former steps to delete it.

(II) When adding an atom, we do so along the direction of charge compensation in the last structure as locally as possible.

(III) All of the operations will accord to a causal relationship.

According to the upper principles, we will construct the D-HA model complying with the following steps:

(1) In this step, we will add a CO_3^{2-} group into the lattice substituting for a PO_4^{3-} group. On the basis of the above statements, we need only put CO_3^{2-} to the PO_4^{3-} location to sustain the initial charge compensation as far as possible. Respectively, we put a carbon atom to each center of the four faces of a PO_4^{3-} tetrahedron occupying three of the four oxygen atoms in PO_4^{3-} to form CO_3^{2-} groups; thus we can obtain four configurations. Next, we perform geometry optimization and energy calculation of the four configurations, respectively, with the other atoms fixed except for the CO_3^{2-} groups. Finally, we

select the one with the lowest total energy in the four configurations and carry out full relaxation with all of the atoms unfixed.

(2) There is an oxygen vacancy in the lattice deriving from step 1. The oxygen atom in this location is coordinated to calcium ions. Therefore, deleting the most affected calcium mainly by oxygen vacancy and lesser by CO_3^{2-} group in close proximity is a wise idea for making a lower energy. In this step, we will calculate the total energy of three possible configurations with Ca vacancy. Finally, the most stable lattice model is obtained, which has one CO_3^{2-} substituting for one PO_4^{3-} and a calcium vacancy in it.

(3) The calcium defect in the last step must impact other oxygen ions coordinated to it. To bond hydrogen ion to the most impacted oxygen ion can further reduce the instability caused by the introduction of hydrogen. In this step, we will add a hydrogen atom respectively to the side of possible oxygen atoms to ascertain where is the most needed hydrogen location. Here, we obtain four possible configurations, for which we perform geometry optimization with other atoms fixed except the added hydrogen atom. The configuration with the lowest total energy then can be found. Finally, we perform geometry optimization to the selected one with all of the atoms unfixed.

(4) Up to now, there are two oxygen atoms that have been defective as compared to the pure HA lattice: one has been deleted; the other has been bonded with H. These two oxygen defections impact the calcium atoms coordinated to them. In this step, we will select the most impacted calcium atoms to delete it. Similarly to step 2, the total energy of the configurations with possible calcium vacancy has been calculated, and finally the most stable configuration is selected.

(5) In this step, we will first add a hydrogen atom to the calcium vacancy (in fact, the calcium is substituted by hydrogen) obtained in step 4, and then perform geometry optimization with other atoms fixed except for this added hydrogen atom. Next, similarly to step 3, we add the other hydrogen atom to the possible oxygen atoms in close proximity. When the most stable configuration is obtained, we perform geometry optimization with all of the atoms unfixed finally.

All through the upper operations, if the atoms are all unfixed, the lattice parameters are also unfixed.

Results and Discussion

Unit Cell Geometry. In this Article, one of the main purposes is to study whether hbs can form and how strong they are between C=O in PLA and hydroxyl in HPO_4^{2-} (P-OH) of D-HA. To facilitate theoretical research, the molecular formula $\text{Ca}_8[(\text{HPO}_4)_3(\text{PO}_4)_2(\text{CO}_3)](\text{OH})_2$ is somewhat subjective to a certain extent. For example, it may be questioned that the CO_3^{2-} contents and the quantities of HPO_4^{2-} groups are slightly higher. In fact, the CO_3^{2-} content can easily achieve a higher level if the alkaline solution is exposed to atmosphere for a long time, and in animal hard tissues this content is also hackneyed. From the view of the charge compensation, OH^- vacancy or substitution by H_2O and Ca^{2+} substituted by Na^+ , K^+ , etc., unit cation comparing with Ca^{2+} vacancy will increase the positive charges in the system. These are not favorable for the formation of HPO_4^{2-} groups. The assumptions in the Experimental Section ignoring these cases are somewhat the reason besides their relative low contents. In fact, this form is more like a surface than a bulk,¹³ although the OH^- content is saturated. Finally, without prejudice to the significance of the study, we obtained the following formula.

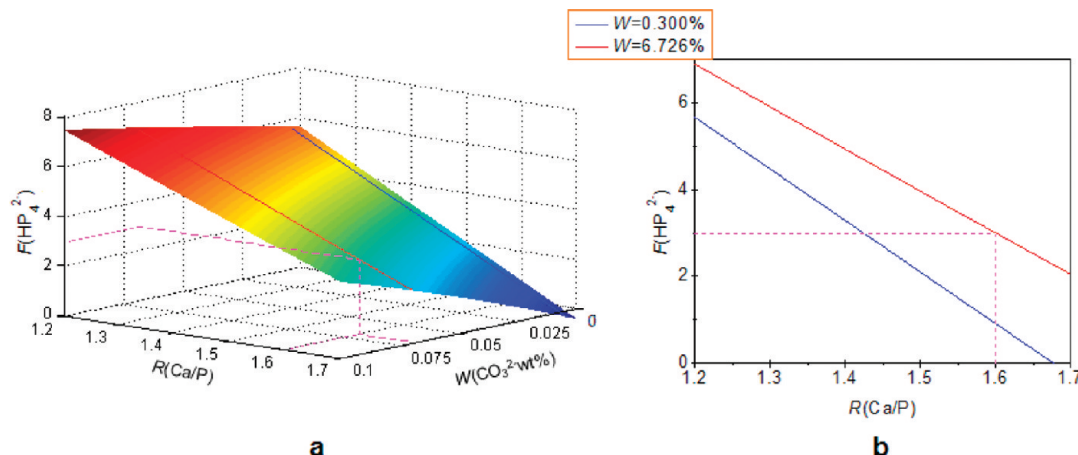


Figure 3. The function (eq 2) graph of the quantities of HPO_4^{2-} in each D-HA lattice. Part a denotes the $F(\text{HPO}_4^{2-})$ varies with $R(\text{Ca}/\text{P})$ and $W(\text{CO}_3^{2-} \text{ wt } \%)$. Part b denotes F varies with only R under $W = 0.3$ wt % and $W = 6.726$ wt %, respectively. It is noteworthy that the globoidal in (a) is deflexed appreciably, so the arc in (b) is deflexed also.

On the basis of the first two equations in eq 1, we can obtain eq 4.

$$F = S(2R - 1) - 12R + 20 \quad (4)$$

Also, on the basis of eq 1, we can derive eq 5.

$$F = \frac{674WR - 360R + 48W + 600}{19WR + 18W + 30} \quad (5)$$

To make partial derivatives to R and W for both sides of eq 5, respectively:

$$\frac{\partial F}{\partial W} = \frac{180(2R - 1)(19R + 52)}{(19RW + 18W + 30)^2} \quad (6)$$

$$\frac{\partial F}{\partial R} = \frac{60(17W - 15)(11W + 12)}{(19WR + 18W + 30)^2} \quad (7)$$

Equation 4 is to say, under a certain Ca/P molar ratio ($0.5 < R < 1.67$), the more quantities of the substitutions of CO_3^{2-} groups for PO_4^{3-} groups, the more quantities of the HPO_4^{2-} groups. From eq 6 we can see that, under the same condition as referred to above, F in eq 5 will increase with W increasing. That is to say, the increasing of CO_3^{2-} quality contents can make the quantities of HPO_4^{2-} in each lattice increase. This is similar but not the same as the above statement. Thus, for the presence of B-type CO_3^{2-} groups in the D-HA lattice, it can make the quantities of HPO_4^{2-} groups increase under a relative higher Ca/P molar ratio (<1.67, i.e., 1.65) than only Ca^{2+} vacancy resulting HPO_4^{2-} groups produced in pure HA. This may also provide a better explanation why the CO_3^{2-} groups in the HA lattice can increase the surface activity of HA. Equation 7 shows that F in eq 5 will increase with R reduced if W is constant and $W < 15/17$. That is to say, the decrease of Ca/P molar ratio can make the quantities of HPO_4^{2-} groups in each lattice increase. Also, from the further analysis, the increase of CO_3^{2-} contents can make the value of $(\partial F)/(\partial R)$ increase a little, so the CO_3^{2-} contents do not impact the trend of F changing with R notably. The statement above can be seen intuitively in Figure 3, which shows the change status of F (in eq 5) with R and W , and (b) is the special cases in $W = 0.300\%$ and $W = 6.726\%$ of (a).

TABLE 1: Relative Total Energy of Different Possible Configurations per Steps^a

steps	E_a (kJ mol ⁻¹)	E_b (kJ mol ⁻¹)	E_c (kJ mol ⁻¹)	E_d (kJ mol ⁻¹)
1	5.51	0	28.00	41.03
2	38.87	17.07	0	
3	0	26.34	19.63	100.21
4	10.09	88.18	82.08	0
5	60.82	37.09	37.09	0

^a Numbers 1–5 denote the steps described in this Article. For convenience, we put the five steps together. E denotes the total energy relative to the most stable configuration in each step. Subscripts a–d mark the possible different configurations in each step. Subscripts a–d correspond to the (a)–(d) in Figures 3–7. In every step, the energy of the most stable configuration is as the 0 kJ mol⁻¹ reference energy.

To benchmark the accuracy of the methods for our calculations, we carried out initial tests on the pure HA system. The relaxed pure HA is shown in Figure 1b. We obtained the lattice constants $a = b = 9.513$ Å, $c = 6.849$ Å, which are in good agreement with the experimental values $a = b = 9.432$ Å, $c = 6.881$ Å,⁵⁸ within 1% error in them. Our calculated results are better than the calculated values $a = b = 9.563$ Å, $c = 6.832$ Å, obtained by de Leeuw⁵⁹ using DFT and little worse than the values $a = b = 9.42$ Å, $c = 6.87$ Å, calculated by Ma et al.⁶⁰ employing DFT too. However, this result we obtained is sufficient for our further study. Furthermore, a plane wave energy cutoff of 700 eV was tested to be sufficient for the description of hbs here.

Now, we will turn to the process of constructing the D-HA model. Table 1 shows all of the relative total energy per system, in which the E_a – E_d correspond to the relative total energy of configurations in the cases of (a)–(d) in Figures 4–8. The model b in Figure 4 is the most stable configuration in step 1. At the same time, we notice that the total energy between models c and d is widely different, whereas it only differs a little between models a and b. We attribute the difference between models a and b to the HA model we used in the hexagonal structure so that the location of CO_3^{2-} in configurations a and b should be equivalent. Here, we obey the result we obtained. From Figure 4, we can see that in discretionary one face of PO_4^{3-} tetrahedron (for example, in Figure 4b and e) the O atoms in CO_3^{2-} will try to be in the location as they are in the PO_4^{3-} to coordinate to Ca^{2+} , through moving slightly to overcome the differences. Also, the deleted O per case seems not to impact the entire HA lattice remarkably. These are all in agreement with our assumption.

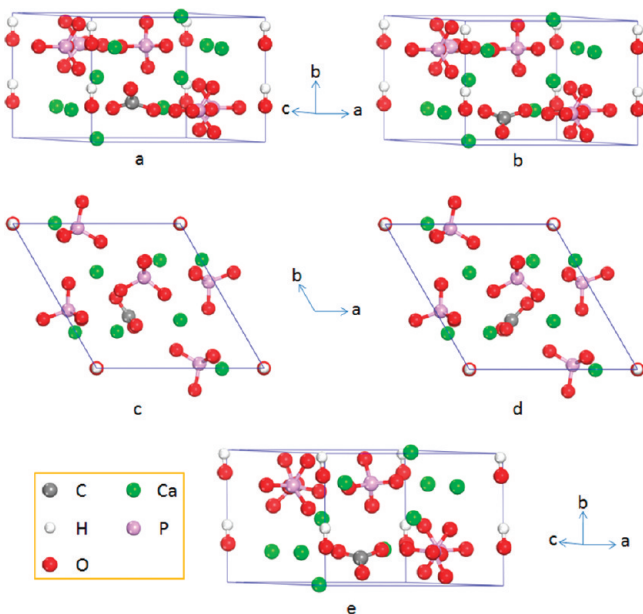


Figure 4. Deficient HA with a CO_3^{2-} on one face of the PO_4^{3-} tetrahedron. (a)–(d) The CO_3^{2-} has been relaxed with other atoms to be fixed. (e) The deficient HA after full relaxation with only CO_3^{2-} in the lattice.

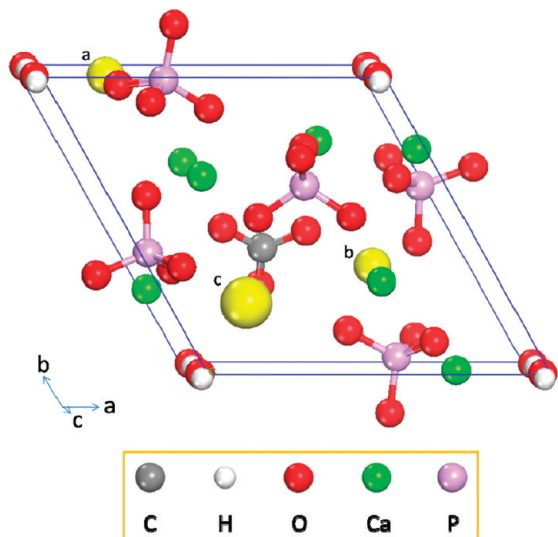


Figure 5. Plane view of deficient HA unit cell with one CO_3^{2-} and three possible Ca deficient locations. The three yellow ions are Ca ions, and the bigger yellow one is the most possible deficient Ca ion.

tions I and II. At the beginning, the aim of fixing the other atoms and permitting the CO_3^{2-} to move freely is to create an environment the same as in the pure HA to fix the CO_3^{2-} compensate location preparatorily and find which O the HA do not need most. This is also based on assumption I. In step 2, there are three possible calcium vacancies, with which the system can retain more stable than with others, as seen in Figure 5. The yellow ones are the possible Ca vacancies; the most stable Ca vacancy is denoted as the bigger yellow one. The relative total energy of each case after deleting Ca atom is listed in Table 1, from which we can see the structure c is the most stable configuration. That is to say, the Ca vacancy in this position with other Ca ions retaining their location can make the lattice more stable than others. Here, the total energy calculation before the full relaxation is still based on the assumption I. Also, deleting the Ca near the O vacancy is based on the assumption II, which we think can decrease the system energy more

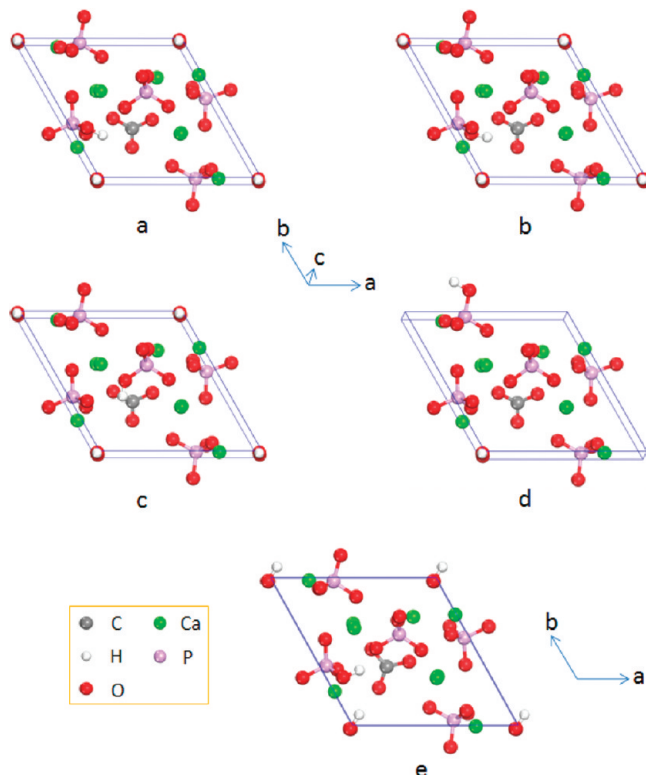


Figure 6. Plane view of deficient HA unit cell with one H and one CO_3^{2-} in the lattice. Parts a–d show the H atoms, which bond to possible O atoms after relaxation with other atoms fixed. Part e shows the full relaxed configuration of the more stable deficient HA cell in (a)–(d).

effectively than deleting others. To add H in step 3, the Ca can be substituted by H first; then the location of H is optimized with other atoms fixed. Unfortunately, we find that the H flies by the OH^- group to form H_2O . This is not what we want. So we make four possible configurations, shown in Figure 6. On the basis of assumption I, the location of added H is optimized with other atoms fixed in each model. The optimized configurations are shown in Figure 6a–d. We find the structure a is the most stable configuration. The relative total energy has been summarized also in Table 1. After the full relaxation, Figure 6e shows the final configuration. This result is not the same as that of Astala et al.,³³ who use a similar method. Their result has been validated also, but the result shows that our configuration is more stable. On the basis of assumption II, to delete the Ca near the O deficient will make the lattice more stable in step 4. Therefore, we delete the possible Ca influenced by O, which bond to H in HPO_4^{2-} in step 3 and the O vacancy in step 1. We have made four possible Ca vacancy configurations, as shown in Figure 7. The relative total energy has been shown in Table 1. Model d is the most stable configuration. Finally, two H atoms will be added into the model. The first H will locate at the Ca vacancy obtained in step 4 (H substitute for Ca), and then the location of the added H is optimized with other atoms fixed. It will fly by the O in PO_4^{3-} . We think that the method of H being selected by O automatically can cause a more stable system. The final configuration is shown in Figure 8a. To add the other hydrogen atom is similar to that in step 3. The three optimized possible configurations are shown in Figure 8b–d. As is shown in Table 1, model d is the most stable configuration. In the end, the full relaxed configuration with all of the atoms unfixed is obtained, as shown in Figure 8e. Additionally, we have verified a group of other cases stochastic-

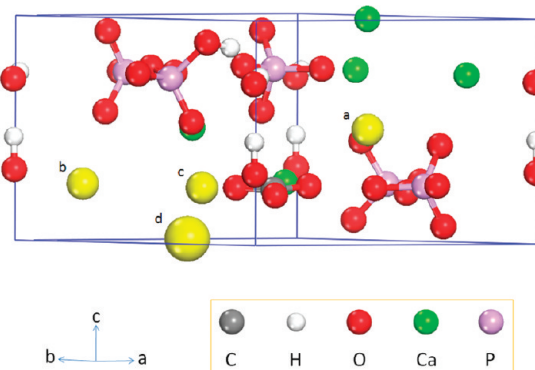


Figure 7. Side view of deficient HA unit cell with one CO_3^{2-} , one HPO_4^{2-} , and four possible Ca deficient locations. The four yellow ions are Ca ions, and the bigger yellow one is the most possible deficient Ca ion.

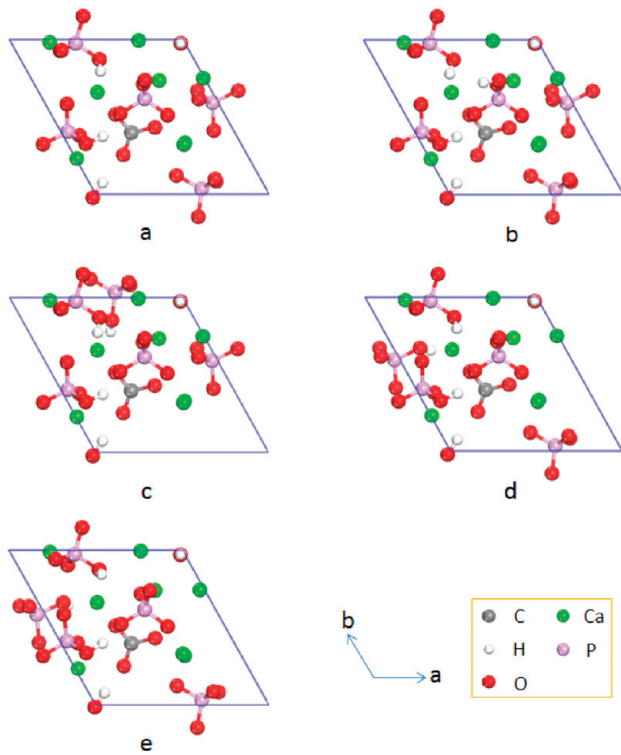


Figure 8. Plane view of deficient HA unit cell with H atoms and one CO_3^{2-} in the lattice. Part a shows the H atoms, which bond to the most possible O atoms after relaxation with other atoms fixed. Parts b–d show the H atoms, which bond to the most possible O atoms after relaxation with other atoms fixed. Part e shows the full relaxed configuration of the more stable deficient HA cell in (b)–(d).

cally; the results show that they are more unstable than our stable configurations.

Figure 9 shows the finally obtained configuration of D-HA, which has three HPO_4^{2-} groups, two calcium vacancies, and one carbonate in it. The lattice parameters are $a = 9.312 \text{ \AA}$, $b = 9.534 \text{ \AA}$, $c = 6.796 \text{ \AA}$; $\alpha = 90.41^\circ$, $\beta = 89.31^\circ$, $\gamma = 119.113^\circ$; and the cell volume is 527.105 \AA^3 . For this system, the a -axis was found to shrink by 2.11%. This was in agreement with the results of Zapanta-LeGeros⁶⁰ who attributed it to the smaller planar CO_3^{2-} group substitutes for the larger tetrahedral PO_4^{3-} group and Astala et al.³³ who utilized DFT to calculate a similar system. The b -axis changed very little, decreasing by only 0.22%. This disagreed with the result of Astala et al. who reported that the b -axis increased. The c -axis expanded by

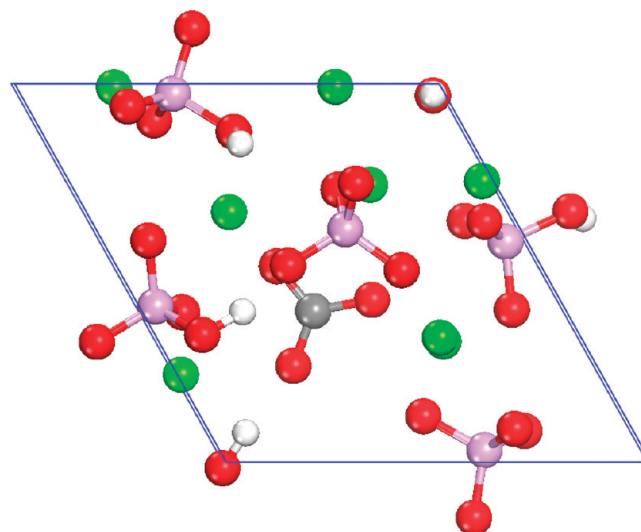


Figure 9. Plane view of full relaxed HA with three HPO_4^{2-} groups, two Ca^{2+} vacancies, and one CO_3^{2-} in the lattice. This configuration is optimized with a $2 \times 2 \times 2 k$ -point.

0.77%, and the unit cell volume decreased by 1.80%. They also agreed with the results obtained by Astala et al. However, the model we studied is not all the same as in the literature, as a comparison with our calculated data is somewhat unreliable.

Of all of the ions/ionic groups in D-HA, the CO_3^{2-} groups are more important. Here, the CO_3^{2-} group retains a planar geometry with $\text{O}-\text{C}-\text{O}$ angle of 118.5° – 121.0° and a bond length of about 1.3 \AA (1.268 , 1.286 , and 1.312 \AA , respectively). The CO_3 plane is close to parallel to the a/b -plane, making an angle of about 1.80° . This is in agreement with the conclusions of Peroos et al.,²⁷ Leventouri et al.,³² and Astala et al.,³³ who have studied a similar system.

In the HPO_4^{2-} groups (Figure 9), the $\text{O}-\text{H}$ distances are 0.994 , 1.031 , and 1.002 \AA , respectively. They are all longer than the two $\text{O}-\text{H}$ distances of 1.001 and 0.973 \AA in channel OH^- groups. The $\text{P}-(\text{OH})$ bond lengths are 1.613 , 1.593 , and 1.590 \AA , respectively. They are all longer than the $\text{P}-\text{O}$ bond length of 1.525 , 1.519 , and 1.152 \AA in pure HA. These results are in agreement to a certain extent with the results of Astala et al.³³ who studied a similar system. The distortion indices of HPO_4^{2-} can be reflected on using the following root-mean-square difference formula 8:

$$D_{\text{RMS}} = \sqrt{\frac{1}{6} \sum_{i=1}^6 (\theta_i - \theta_0)^2} \quad (8)$$

This formula can measure the deviation of the six $\text{O}-\text{P}-\text{O}$ angles (θ_i) from the ideal tetrahedron value [$\theta_0 = 180 \cos^{-1}(-1/3)/\pi$]. The three HPO_4^{2-} had been measured to have deviation values of 4.21 , 2.60 , and 2.17 , respectively. The three $(\text{PO})-\text{H}$ bond lengths are 1.031 , 1.002 , and 0.994 \AA , respectively.

The angles between OH^- groups and a/b -plane are 17.46° and 88.71° , respectively. One of the two OH^- groups in the lattice is also a notable feature; it is initially parallel to the c -axis and now points almost parallel to the a/b -plane, which agrees with Astala et al.³³ who attributed it to the stem from electrostatic interactions, with the positive end of the OH dipole approaching the negative Ca vacancy.

(001) Surface. Here, we do not think that atom rearrangement of breaking chemical bonds can make a more stable surface.

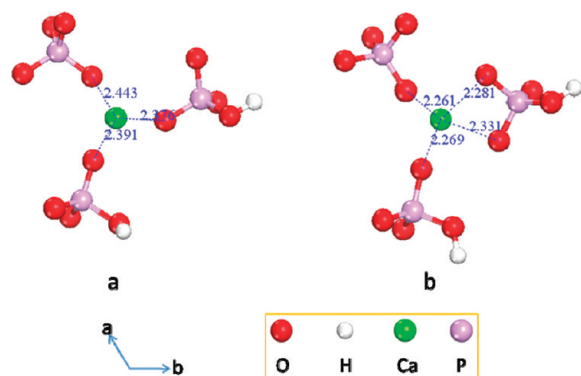


Figure 10. The partial surface configuration of the D-HA (001) surface. (a) Initial; (b) final.

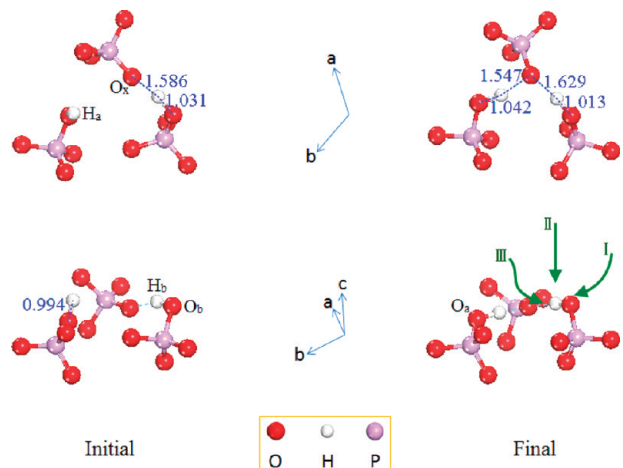


Figure 11. The partial surface configuration of D-HA. The upper and lower parts correspond to the same configuration seen from different views; the left and right parts are the initial and final configurations, respectively.

After relaxation, the slab thickness increases by 0.534 Å, and the unfixed slab thickness increases by 7.040%. The Ca (here we only study the Ca(I)) is seen to move into the surface for it has dropped 0.362 Å as compared to the most top O in surface HPO_4^{2-} . In fact, it has dropped 0.152 Å vertically, and moved 0.336 Å corresponding to the initial location. The distance between this Ca and the one in the second layer below has held the line. The Ca in the second layer has dropped a little, only 0.002 Å, and moved 0.456 Å relative to the initial location, which is more moved than the top Ca, mainly caused by the moved location of CO_3^{2-} . The distance between the second layer Ca and third layer Ca increased 0.022 Å. After relaxation, the coordinate number of surface Ca by O bonding to $\text{PO}_4^{3-}/\text{HPO}_4^{2-}$ group has changed from three to four (Figure 10). This remarkably decreased the charge on calcium ion. From eq 8, the deviation values of the surface three $\text{HPO}_4^{2-}/\text{PO}_4^{3-}$ groups are 4.054, 3.846, and 1.942 Å, respectively. The angle between CO_3^{2-} plane and a/b -plane has become 30.39°, and between OH^- group and the c -axis has become -3.54°. The OH^- group has pointed to one O in CO_3^{2-} with the $\text{H}\cdots\text{O}$ distance of 2.249 Å. The H (H_a) atom in the surface HPO_4^{2-} has fallen into the surface and become flat from upright (Figure 11).

To describe it clearly, we labeled some atoms at first, which can be identified in Figure 11. We labeled two H atoms as H_a , H_b and three O atoms as O_x , O_a , and O_b , of which H_a bonds with O_a and H_b bonds with O_b , respectively; I, II, III are the path of C=O attacking the H_b , of which II is from top, and I and III are from hollow. From the final configuration in Figure

11, we can see that the O_a-H_a bond length of 1.042 Å is longer than the O_b-H_b bond length of 1.013 Å. The prime reason is that there are two Ca absent, which are coordinate to O_b in the pure HA, and only one to O_a . So O_b is more active than O_a , which made the bond length of O_b-H_b shorter. On the contrary, it is interesting that the distance of $\text{H}_a\cdots\text{O}_x$ is shorter than $\text{H}_b\cdots\text{O}_x$. Through further analyses, we found that this resulted mainly by the joint actions of the directivity of the electron orbits of O-2p and the force field produced by other atoms/atomic groups nearby them. Besides to fold with the P-sp³ hybrid orbitals to form the P-O bond, the rest of the O-2p is also directivity, which makes the electron density in the ring zone of about 115° with P-O bond higher than in other directions. Also, H-1s is mainly in this direction to form a σ bond with O-2p. In the force field generated by other atoms, the final angle of $\text{P}-\text{O}_x\cdots\text{H}_a$ becomes about 105.7°, and $\text{P}-\text{O}_x\cdots\text{H}_b$ becomes about 152.1°. Therefore, H_a have a stronger attraction from O_x than H_b , which make the $\text{H}_a\cdots\text{O}_x$ distance of 1.547 Å shorter than $\text{H}_b\cdots\text{O}_x$ of 1.629 Å. This is also one of the reasons that the bond length of O_a-H_a is longer than O_b-H_b .

Adsorptions. Here, we studied the PLA model (methyl lactate) adsorption on the D-HA (001) surface. In the actual system, due to the temperature and pressure, the C=O may get enough energy to close to the active points. Here, we only investigate these cases. We have placed C=O in all possible positions, involving the top and the hollow. We also consider the steric resistance of other atoms in PLA model and D-HA surface and try to decrease these influences, and also care about the activity position of the highest and the lowest in C=O. The activity position of D-HA surface and PLA model can be seen intuitively in Figure 12a,b. We found that it is easy for C=O to capture H_a , and difficult or impossible to capture H_b . This is also perplexed in that the distance of $\text{H}_a\cdots\text{O}_x$ is shorter than $\text{H}_b\cdots\text{O}_x$. For this phenomenon, we give the following interpretation. From a macro point of view, the atoms in the surface always have a tendency to come back to the position as it is in the stable D-HA lattice. Because the formation of (001) surface does not destroy the stable structure in the crystal, there is less tendency for H_b to escape outside of the D-HA surface to be captured by C=O. However, the formation of (001) surface has made H_a come to a location catching by O_x . It is not a more enjoyable location for H_a , or else in the crystal it would have been caught by O_x . In case of a suitable condition, the H_a atom will escape outside back to the original position in the crystal as far as possible. From Figure 15, we can see that the caught H by C=O had come back to the approximate location as it is in the lattice (Figures 9 and 11). From a micro point of view, we also attribute it to the joint action of the directivity of the electrons orbits of O-2p and the influence of other atoms/atomic groups near to them. For the C=O to capture H from HPO_4^{2-} is an adventure in that the other O nearby will exclude it to the outside of the surface. Therefore, once the C=O has captured the H, it will endeavor to haul it out. If the C=O attacks H_b along path I, because of the directivity of the electron orbits of O-2p, H_b needs to transit along a concave arc path or the O_b shift location to fit it to be pulled out, as shown in Figure 13a. This is either difficult or impossible for C=O. During our calculation, we found that the instant capture of H_b made the H_a move from O_a to O_x ; this can be seen in Figure 13a(2-3). This is mainly because two Ca have been absent, which are coordinate to O_x . If there is no H_b to balance it, the O_x would become more active than O_a . Finally, the C=O fails to capture anything (Figure 13a(3)). If the C=O attacks H_b along path II, for the same reason as above, H_b being directly dragged up is

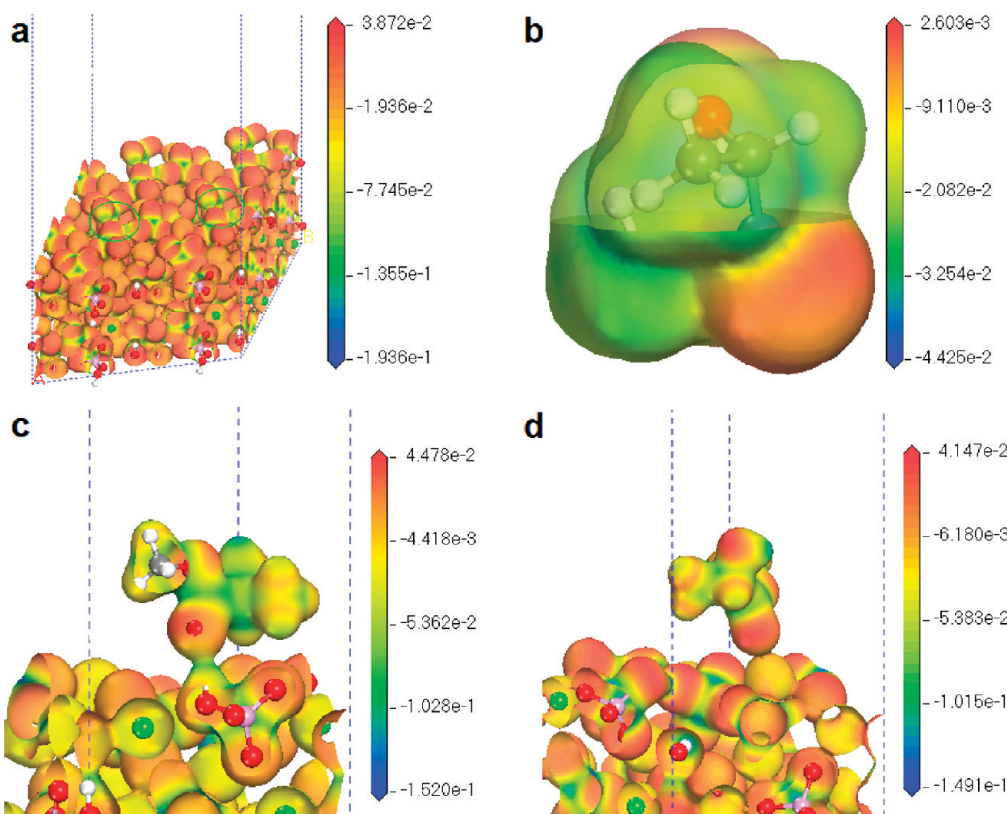


Figure 12. The electron density. (a) The relaxed (001) surface of D-HA. (b) The PLA model. (c) The PLA model interacting with P-OH. (d) The PLA model interacting with Ca. The green ellipses in (a) denote the P-(OH) active positions.

also difficult or it is the case similar to that along path I, and this can be seen in Figure 13b. If the C=O attacks H_b along path III, C=O can get the maximum probability to capture H_b. However, unfortunately, it cannot. This can be seen in Figure 13c. The ability of C=O and the pull produced by other atoms/atomic groups nearby them to add up together also cannot overcome O_x. During this process, the C=O is nearby the H_a, too (Figure 13c(2-3)). H_a along this direction has exposed more positive charge (Figure 11). Also, for the directivity of O-2p, the action of C=O pulling out H_b will make C=O more close to H_a; the exclusion of O_b and O_x will also make C=O close to H_a. Meanwhile, the C=O to allure H_a will make O_x more active. This can make the O_x more firmly grasp H_b not to allow the C=O capturing it (Figure 13c). For the same reasons as above, it is easier for C=O to capture H_a in this side than in the top position and on the other side. Moreover, besides these reasons, the formation of O_a-H_a...O_x has made a great tension for the directivity of the electron orbits of O-2p also. To add up the force afforded by other atoms/atomic groups nearby them, finally, the C=O captured the H_a successfully. All of these can be seen in Figure 13d-f (d, the hollow position; e, the top position; f, the other hollow position, C=O has failed). The zone in which C=O can capture H_a has been shown in Figure 14b.

Moreover, on the basis of the upper analyses, we can achieve that there must be more H in the surface that cannot be captured by C=O with the further decrease of Ca/P molar ratio. We also calculated the case with a higher Ca/P molar ratio. The C=O can easily capture the H bonding to PO₄³⁻. Even the H cannot be captured by O in other PO₄³⁻ after the surface relaxation for the existence of other Ca²⁺ nearby, or P-OH gives the H to C=O. Figure 13g(1) shows this case, in which the Ca(I) on the (001) surface has been deleted with H being added to a random

location. However, if the H located the site of charge compensation, in this case, to be captured by C=O is also easy.

Furthermore, we added H_a to O_x and other reasonable O's; also, the H_a can be captured by C=O and H_b cannot. Here, we only calculated one case of the C=O adsorption on the surface Ca²⁺ (Figure 13g(2-3)), through which we could compare the case with H...O. The position at which the C=O can capture is shown in Figure 14b also.

Here, we selected one of the finally stable configurations of adsorption, as seen in Figure 15. To see it clearly, we deleted the outlying atoms in D-HA. The surface atoms of D-HA are in the bottom of the figure, and the PLA model is on the top. According to Bondi,⁶¹ when the interatomic distances are less than the sum of the van der Waals radii, it can be regarded as hbs formed. The radii used in this study are H 1.20 and O 1.52, respectively. On the basis of this, we find a medium strong C-O...H-(OP) hydrogen bond (hb) and two weak strong C-H...O hbs, seen in Figure 15. The bond length, bond energy, and the angle of O-H-O/O-H-C have been displayed clearly in Table 2. To further prove our points, we have done electron density and partial density of state (PDOS) to the final adsorption configuration. From Figure 12c, we can clearly see that the electron density between C=O and H-(OP) has fold. However, there is a gap between C-H and O-P, between which are mainly electrostatic adsorption, weak hbs. In Figure 16a, we present the PDOS of the correlative O and H atoms. As can be expected, the resonances are found in the vicinity of -12.5 eV between O-2p in C=O and H-1s in P-OH orbitals, which is generally interpreted as evidence of hydrogen bonding of nonbonded atoms. However, in Figure 16b and c, there is not a resonance. These also verify our upper arguments. These results are in agreement with the results in the literature.⁶²

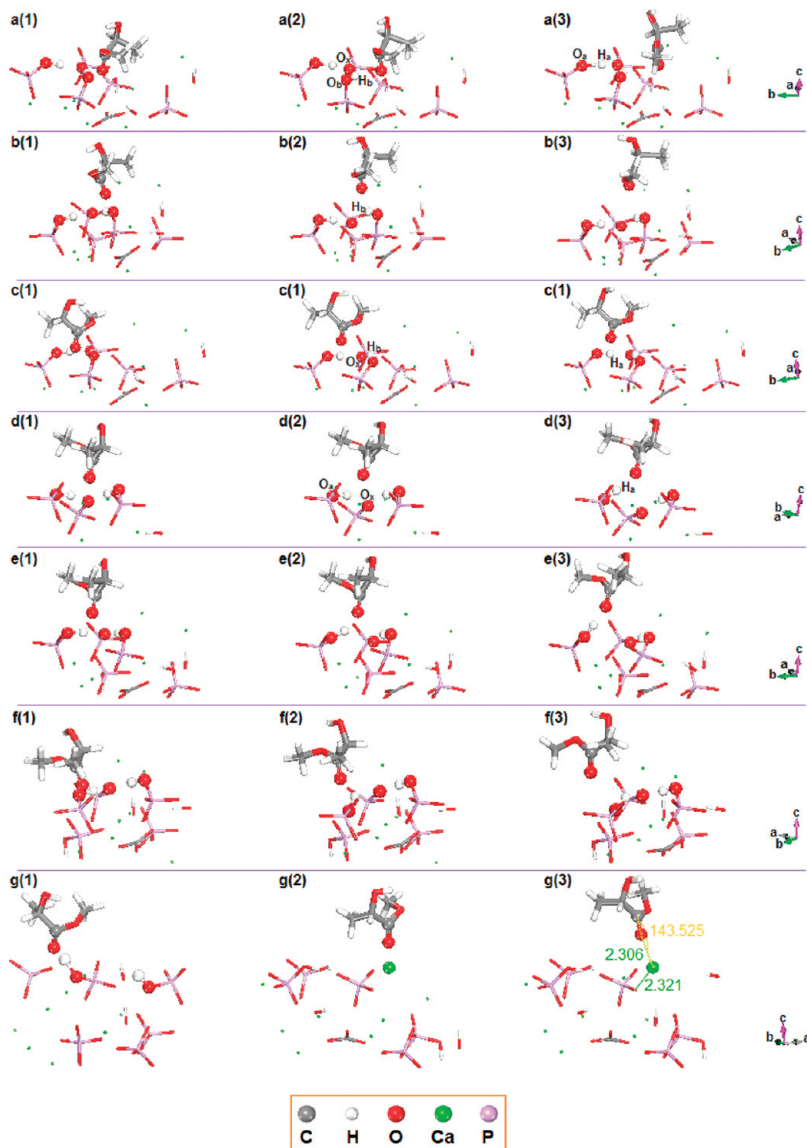


Figure 13. The diversified cases of PLA model on the (001) surface of D-HA. In each row except for g, 1 denotes the initial configuration, 2 denotes configuration in the intermediate process, 3 is not the final configuration, but from 3 we can descry the trend to the final configuration.

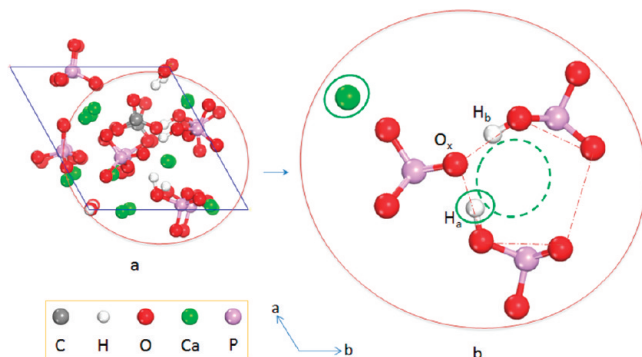


Figure 14. The possible locations where $\text{C}=\text{O}$ could capture H_a and Ca . Part b is a magnified view of (a), which has deleted the impossible atoms. The green dashed ellipse denotes the hollow position that the $\text{C}=\text{O}$ can capture H_a , and the green solid ellipse shows the top position that the $\text{C}=\text{O}$ can capture Ca or H_a .

We also analyzed the electron density of $\text{C}=\text{O}\cdots\text{Ca}$; it is as in the $\text{C}=\text{O}\cdots\text{H}-(\text{OP})$ that the electron density between $\text{C}=\text{O}$ and Ca has fold. To further make clear the interaction substance, we also analyzed the PDOS of C atom and O atom in $\text{C}=\text{O}$, and the Ca . In Figure 17a-c are the DOS of $\text{Ca}-3s3p3d$, $\text{O}-2s2p$,

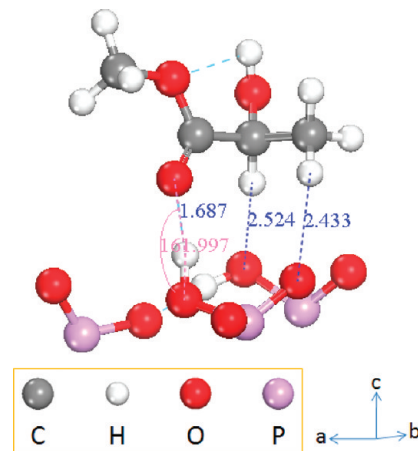


Figure 15. The final configuration of PLA model on the D-HA surface.

and $\text{C}-2s2p$ orbitals. Here, we mainly care about the PDOS of $\text{O}-2p$ and $\text{Ca}-3d$ (Figure 17d). There is a palpable resonance, but not intensity. It means that the electrons are mainly in $\text{O}-2p$ orbitals, and only a little are in $\text{Ca}-3d$. That is to say it is a strong

TABLE 2: PLA/D-HA Interaction Data^a

bonding type	length (Å)	angle (deg)	energy (kJ mol ⁻¹)	essential
O _C ···H _O	1.687	162.0	48	hydrogen bond
O _P ···H _C	2.433	150.9		electrostatic
1	2.524	166.3	average ⁹	
2	2.306	143.5	124	coordination

^a O_C denotes carbonyl oxygen (C=O), O_P denotes oxygen in PO₄³⁻/HPO₄²⁻, and H_O denotes hydrogen in HPO₄²⁻(P-OH).

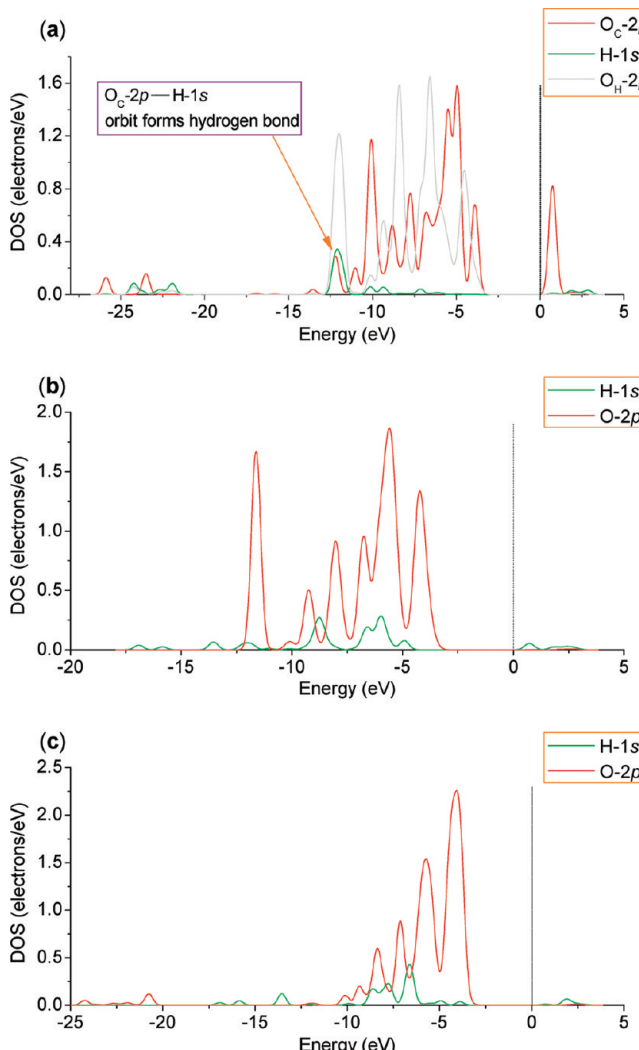


Figure 16. The PDOS of the O-2p and H-1s. Dotted vertical lines correspond to the Fermi level. Part a shows O atom in C=O and H atom in D-HA. Part b shows O atom in HPO₄²⁻ group and H atom in methylene. Part c shows O atoms in HPO₄²⁻ group and H atom in methyl.

ion interaction, with little covalent ingredient between C=O and Ca²⁺. To make it clear, we also obtained the Mulliken charge. The Mulliken charge of Ca has changed from 1.44e to 1.41e, and O has changed from -0.55e to -0.60e. This also certifies a feeble electron transfer from O to Ca.

Moreover, the CH₄ adsorption on the D-HA surface has also been calculated. The aim to perform this task is that we want to obtain the hbs between C-H and P-O to estimate the bonding energy and the bonding angle in the PLA/D-HA system. We obtained the hbs bonding energy as about 9 kJ mol⁻¹, with a bonding angle of about 170°. This angle warps a lot from the C-H···O-P; however, the bond length is almost the same as

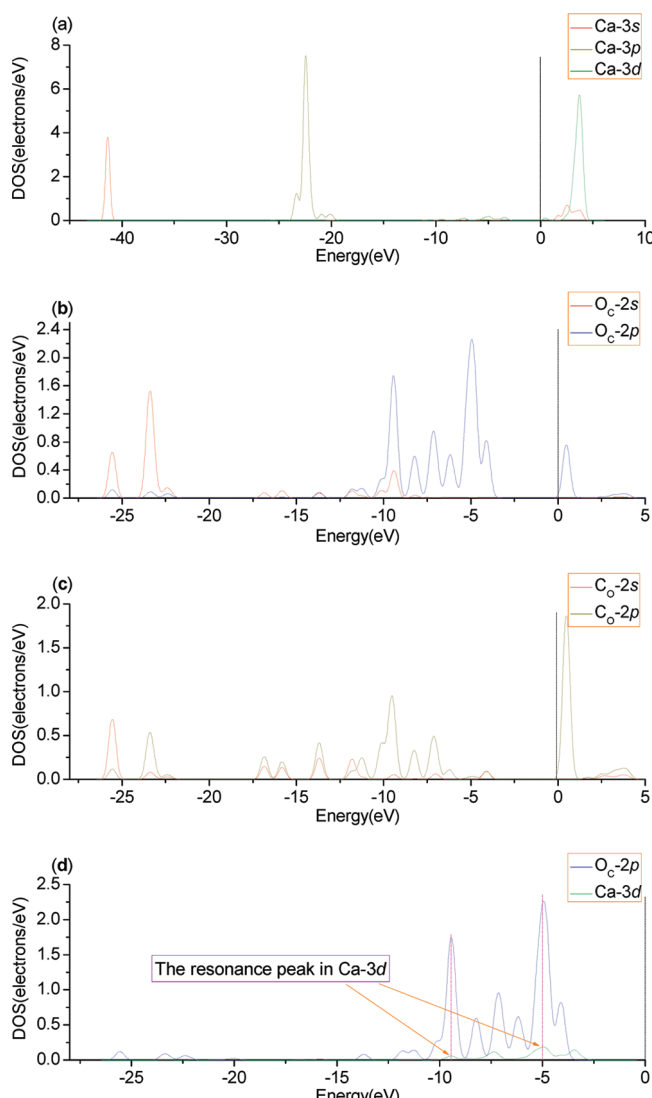


Figure 17. The PDOS of PLA model on the D-HA surface. (a) Ca-3s3p3d, (b) O-2s2p in O···C, (c) C-2s2p bonding to O, and (d) O-2p and Ca-3d in O···Ca.

the C-H···O-P bond. According to Steed et al., the bonding angle is very important for the bonding energy: with increasing deviation from a linear D-H···A arrangement, the accuracy of the DFT-PBE decreases. Therefore, the C-H···O-P angle of 170° and a 700 eV energy cutoff are enough to accurately describe the hbs.⁶³

It is worth noting that we did not study the cases in which H₂O participates in the interaction of PLA and D-HA in the above investigation. However, in most of the synthetic composites, H₂O is often ubiquitous and cannot be fully avoided for that the drying methods are always not absolutely ideal and the water in the environment will also incorporate during storage and usage. In the composites of PLA/D-HA in this Article, the electronegativity of O in H₂O is greater than that in C=O of PLA (in H₂O, -0.71e; in C=O, -0.44e); and the electron positivity of H in H₂O is also greater than in methyl/methylene (in H₂O, 0.35e; in methyl/methylene, 0.11–0.16e). Thus, we conjecture that in many cases the water could be priority to hold the D-HA surface than PLA. At the same time, the binding energy between C=O in PLA and H in H₂O is 28 kJ mol⁻¹, which is lower than the binding energy between C=O in PLA and H in HPO₄²⁻(48 kJ mol⁻¹). So, we conjecture that the presence of water is not beneficial for the activity of the

nanoparticles to PLA, and in the actual instances the interaction effects are more or less no better than in our calculations. In view of the complexity of studying all situations, we have chosen to investigate a simple and more representative situation amply in this Article.

Conclusions

A more actual D-HA surface has been constructed, and the interaction mechanism between PLA and the (001) surface of D-HA has been investigated employing DFT. The results show that hbs can form between PLA and the surface of D-HA, mainly the hbs between C=O and P-OH. They are medium strong hbs, with a bond length of about 1.69 Å, and bond energy of about 48 kJ mol⁻¹. Beside the hbs, C=O in PLA can also interact with Ca, and the binding energy is about 124 kJ mol⁻¹. This Article offers a reference to construct deficient structure according to a certain impurity concentration and to simulate the organic adsorption on deficient lattice surface by means of first principles.

Acknowledgment. This work was partially supported by the National Natural Science Foundation of China (50773065), Programs for New Century Excellent Talents in university, Ministry of Education of China (NCET-07-0719), and Sichuan Prominent Young Talent Program (08ZQ026-040).

References and Notes

- (1) Wang, H.; Li, Y.; Zuo, Y.; Li, J.; Ma, S.; Cheng, L. *Biomaterials* **2007**, *28*, 3338.
- (2) Alexandre, M.; Dubois, P. *Mater. Sci. Eng.* **2000**, *28*, 1.
- (3) Zhou, S. B.; Zheng, X. T.; Yu, X. J.; Wang, J. X.; Weng, J.; Li, X. H.; Feng, B.; Yin, M. *Chem. Mater.* **2007**, *19*, 247.
- (4) Gain, O.; Espuche, E.; Pollet, E.; Alexandre, M.; Dubois, P. J. *Polym. Sci., Part B: Polym. Phys.* **2005**, *43*, 205.
- (5) Gorassi, G.; Tortora, M.; Vittoria, V.; Pollet, E.; Alexandre, M.; Dubois, P. J. *Polym. Sci., Part B: Polym. Phys.* **2004**, *42*, 1466.
- (6) Shikinami, Y.; Okuno, M. *Biomaterials* **2001**, *22*, 3197.
- (7) Choi, D.; Marra, K. G.; Kumta, P. N. *Mater. Res. Bull.* **2004**, *39*, 417.
- (8) Schiller, C.; Epple, M. *Biomaterials* **2003**, *24*, 2037.
- (9) Kokubo, T.; Kim, H. M.; Kawashita, M. *Biomaterials* **2003**, *24*, 2161.
- (10) Liao, S. S.; Cui, F. Z.; Zhang, W.; Feng, Q. L. *Biomed. Mater. Res., Part B* **2004**, *69*, 158.
- (11) Kim, S. S.; Park, M. S.; Jeon, O.; Choi, C. Y.; Kim, B. S. *Biomaterials* **2006**, *27*, 1399.
- (12) Tanaka, H.; Yasukawa, A.; Kandori, K.; Ishikawa, T. *Colloids Surf., A* **1997**, *125*, 53.
- (13) Cheng, Z. H.; Yasukawa, A.; Kandori, K.; Ishikawa, T. *Langmuir* **1998**, *14*, 6681.
- (14) Wang, X.; Li, Y.; Wei, J.; de Groot, K. *Biomaterials* **2002**, *23*, 4787.
- (15) Nikolenko, N. V.; Esajenko, E. E. *Adsorpt. Sci. Technol.* **2005**, *23*, 543.
- (16) Nikolenko, N. V.; Kuprin, V. P.; Ivanova, M. V.; Taran, I. B. *Colloid J.* **2001**, *63*, 595.
- (17) Misra, D. N. *Colloids Surf., A* **1998**, *141*, 173.
- (18) Pasteris, J. D.; Wopenka, B.; Freeman, J. J.; Rogers, K.; Valsamis-Jones, E.; van der Houwen, J. A. M.; Silva, M. J. *Biomaterials* **2004**, *25*, 229.
- (19) Kay, M. I.; Young, R. A. *Nature* **1964**, *204*, 1050.
- (20) Mostafa, N. Y.; Brown, P. W. *J. Phys. Chem. Solids* **2007**, *68*, 431.
- (21) Elliott, J. C.; Mackie, P. E.; Young, R. A. *Science* **1973**, *180*, 1055.
- (22) Haverty, D.; Tofail, S. A. M.; Stanton, K. T.; McMonagle, J. B. *Phys. Rev. B* **2005**, *71*, 094103.
- (23) Elliott, J. C. *Structure and Chemistry of the Apatites and Other Calcium Orthophosphates*; Elsevier: Amsterdam, 1994.
- (24) Bigi, A.; Cojazzi, G.; Panzavolta, S.; Ripamonti, A.; Roveri, N.; Romanello, M.; Noris Suarez, K.; Moro, L. *J. Inorg. Biochem.* **1997**, *68*, 45.
- (25) LeGeros, R. Z. *Nature* **1965**, *206*, 403.
- (26) Suetsugu, Y.; Takahashi, Y.; Okamura, F. P.; Tanaka, J. *J. Solid State Chem.* **2000**, *155*, 292.
- (27) Peroos, S.; Du, Z.; de Leeuw, N. H. *Biomaterials* **2006**, *27*, 2150.
- (28) Zapanta-LeGeros, R. *Calcium Phosphates in Oral Biology and Medicine*; Karger: New York, 1991.
- (29) Wilson, R. M.; Elliott, J. C.; Dowker, S. E. P.; Smith, R. I. *Biomaterials* **2004**, *25*, 2205.
- (30) Ivanova, T. I.; Frank-Kamenetskaya, O. V.; Kol'tsov, A. B.; Ugolkov, V. L. *J. Solid State Chem.* **2001**, *160*, 340.
- (31) Fleet, M. E.; Liu, X. *Biomaterials* **2007**, *28*, 916.
- (32) Leventouri, T.; Chakoumakos, B. C.; Papaneachou, N.; Perdikatis, V. *J. Mater. Res.* **2001**, *16*, 2600.
- (33) Astala, R.; Stott, M. J. *Chem. Mater.* **2005**, *17*, 4125.
- (34) Ducheyne, P.; Radin, S.; King, L. *J. Biomed. Mater. Res.* **1993**, *27*, 25.
- (35) Perdew, J. P.; Burke, K.; Ernzerhof, M. *Phys. Rev. Lett.* **1996**, *77*, 3865.
- (36) Kresse, G.; Furthmuller, J. *Phys. Rev. B* **1996**, *54*, 11169.
- (37) Fischer, T. H.; Almlöf, J. *J. Phys. Chem.* **1992**, *96*, 9768.
- (38) Mostafa, N. Y.; Brown, P. W. *J. Phys. Chem. Solids* **2007**, *68*, 431.
- (39) de Leeuw, N. H. *Chem. Commun.* **2001**, 1646.
- (40) Mkhonto, D.; de Leeuw, N. H. *J. Mater. Chem.* **2002**, *12*, 2633.
- (41) Ma, X.; Ellis, D. E. *Biomaterials* **2008**, *29*, 257.
- (42) Zahn, D.; Hochrein, O. *Phys. Chem. Chem. Phys.* **2003**, *5*, 4004.
- (43) Zhou, H. L.; Wu, T.; Dong, X. L.; Wang, Q.; Shen, J. W. *Biochem. Biophys. Res. Commun.* **2007**, *361*, 91.
- (44) Shen, J. W.; Wu, T.; Wang, Q.; Pan, H. H. *Biomaterials* **2008**, *29*, 513.
- (45) Zhu, W. H.; Wu, P. *Chem. Phys. Lett.* **2004**, *396*, 38.
- (46) Driessens, F. C. M.; Verbeeck, R. M. H.; Kickens, P. *Anorg. Allg. Chem.* **1983**, *504*, 195.
- (47) Brown, W. E.; Chow, L. C. A new calcium phosphate, water-setting cement. In *Cements Research Progress*; Brown, P. W., Ed.; American Ceramic Society: Westerville, OH, 1987; p 351-79.
- (48) Mkukuma, L. D.; Skakle, J. M. S.; Gibson, I. R.; Imrie, C. T.; Aspden, R. M.; Hukins, D. W. L. *Calcif. Tissue Int.* **2004**, *75*, 321.
- (49) Wu, Y.; Glimcher, M. J.; Rey, C.; Ackerman, J. L. *J. Mol. Biol.* **1994**, *244*, 423.
- (50) Greish, Y. E.; Bender, J. D.; Lakshmi, S.; Brown, P. W.; Allcock, H. R.; Laurencin, C. T. *Biomaterials* **2005**, *26*, 1.
- (51) Wilson, R. M.; Elliott, J. C.; Dowker, S. E. P. *Am. Mineral.* **1999**, *84*, 1406.
- (52) Leventouri, Th. *Biomaterials* **2006**, *27*, 3339.
- (53) Fleet, M. E.; Liu, X. *J. Solid State Chem.* **2003**, *174*, 412.
- (54) LeGeros, R. Z.; Trauz, O. R.; Legeros, J. P.; Klein, E.; Shirra, W. P. *Science* **1967**, *155*, 1409.
- (55) Bonel, G. *Ann. Chim.* **1972**, *7*, 65.
- (56) Elliott, J. C.; Bonel, G.; Trombe, J. C. *J. Appl. Crystallogr.* **1980**, *13*, 618.
- (57) Calderín, L.; Stott, M. J.; Rubio, A. *Phys. Rev. B* **2003**, *67*, 134106-1.
- (58) Posner, A. S.; Perloff, A.; Diorio, A. F. *Acta Crystallogr.* **1958**, *11*, 308.
- (59) de Leeuw, N. H. *J. Chem. Soc., Chem. Commun.* **2001**, *17*, 1646.
- (60) Zapanta-LeGeros, R. *Nature* **1965**, *206*, 403.
- (61) Bondi, A. *J. Phys. Chem.* **1964**, *68*, 441.
- (62) Steed, J. W.; Atwood. *Supramolecular Chemistry*; John Wiley & Sons, Ltd.: England, 2000.
- (63) Ireta, J.; Neugebauer, J.; Scheffler, M. *J. Phys. Chem. A* **2004**, *108*, 5692.